Diego E. Boldrini, Gabriela M. Tonetto* and Daniel E. Damiani

# Overall Effectiveness Factor for Slab Geometry in a Three-Phase Reaction System

**Abstract:** The overall effectiveness factor for slab geometry applicable to uniform washcoats on a monolith surface for three-phase reaction systems was studied in the present work. Analytical solutions for zero-order reactions and Langmuir–Hinshelwood and power law kinetics were reported. The analysis of the theoretical results showed that not considering the geometry of the monolithic system in a proper way lead to 14% errors in reactions parameters when operating under mixed control (kinetic-internal diffusion) and negligible external mass-transfer resistances.

**Keywords:** overall effectiveness factor, monolithic catalyst, slab geometry, three-phase reaction, mass transfer, linear and nonlinear kinetics

## 1 Introduction

Monolithic catalysts have received much interest recently due to their performance in multi-phase catalytic applications [1–3]. Hydrogenation reactions have received special attention given that monoliths have excellent characteristics associated with mass transport, and many of those reactions are hindered by this phenomenon. For many hydrogenation reactions, currently used conventional reactors are based on slurry systems operated in batch or semi-batch mode. Even though this technology has been used for decades by the industry, it has several disadvantages [3], the most important of which is the difficulty to separate the suspended powder catalyst from the reactant mixture after the reaction. In the particular case of the hydrogenation of vegetable oils, the contribution of the filtering and purification stages to the overall costs of the process is usually significant, representing about 20% of the total operating costs, and as much as 50% if the consumption of hydrogen and catalyst are excluded [4].

Various alternative designs based on monolithic systems have been proposed as potential solutions to simplify the process [5–9]. Monolithic catalysts have been used in aqueous-phase hydrogenation reactions, such as 2-ethyl-hexanol [10], α-methylstyrene and benzaldehyde [7, 11], butene-1,4-diol [12], and vegetable oils [4, 13–16], among others. In all these works, the operating advantages were pointed out, such as the easy separation of the catalyst and purification of the products, mixing requirements, and better selectivities resulting from a better mass-transfer performance [17].

A monolithic catalyst consists of a structure made of a ceramic or metallic substrate, and it has the shape of a block with multiple channels. Generally these channels are parallel and have a honeycomb configuration [1].

The presence of external and internal diffusional limitations has been described in many practical situations, catalytic hydrogenation in particular, and many three-phase catalytic reactions in general, where high reaction rates and temperatures prevail [18–21]. A three-phase reaction system implies a variety of stages, such as gas–liquid mass transfer, liquid–solid mass transfer, intraparticle diffusion, and chemical reaction. A concept that was developed some time ago, mostly for catalysts having spherical geometries, is the overall effectiveness factor, which considers the effects of all the transport resistances, either internal or external [22, 23]. For honeycomb catalysts, a uniformly distributed active coating in the internal walls of the monolith channel can be assumed. In this case, a simple slab geometry of the catalyst could be considered.

The aim of the present work was to develop analytically the overall effectiveness factor for slab geometry applicable to uniform washcoats on monolithic surfaces for three-phase reaction systems, valid for linear and nonlinear kinetics.

*Corresponding author: Gabriela M. Tonetto, Department of Chemical Engineering, PLAPIQUI-UNS CONICET, Bahía Blanca, Buenos Aires 8000, Argentina, E-mail: gtonetto@plapiqui.edu.ar
Diego E. Boldrini: E-mail: dboldrini@plapiqui.edu.ar,
Daniel E. Damiani: E-mail: ddamiani@plapiqui.edu.ar, Department of Chemical Engineering, PLAPIQUI-UNS CONICET, Bahía Blanca, Buenos Aires 8000, Argentina

# 2 Theoretical background: overall effectiveness factor

In many cases, the concentration of the liquid reactant is greatly in excess of that of the dissolved gas. The analysis in this work refers to the situation where the gas species ($G$) is the limiting reactant.

The concept of overall effectiveness factor was first introduced to simplify the calculation of the reaction rate in three-phase systems [24], and then it was extended to nonlinear systems [23, 25]. This concept has the advantage that all the relevant parameters can be organized into conveniently defined dimensional groups. In this way, the results could be represented graphically. These plots remove the need for trial-and-error calculations for the reaction rate.

The overall effectiveness factor, for a three-phase reactor, is defined as the ratio of the observed reaction rate ($R_G$) to the reaction rate without transport resistances ($\Omega_G$) according to the following equation:

$$= \frac{R_G}{w \cdot \Omega_G(G^*)} \tag{1}$$

where

$$R_G = M_G \cdot (G^* - G_S) \tag{2}$$

$$\frac{1}{M_G} = \frac{1}{k_{GL} \cdot a_L} + \frac{1}{k_{LS} \cdot a_S} \tag{3}$$

It is worth noting that $\Omega_G$ will be expressed according to the type of kinetics adopted. When the reactor operates at maximum efficiency, $\eta$ tends to unity and it decreases in the presence of transport resistances.

In order to obtain an analytical solution for $\eta$ in terms of known parameters, the concentration of $G$ on the surface ($G_S$) is redefined. This is done by defining this concentration as a function of the overall effectiveness factor. From eq. (2) and the definition of $\eta$ given by eq. (1), we obtain

$$G_S = G^* \cdot \left(1 - \frac{\eta}{\sigma_G}\right) \tag{4}$$

where

$$\sigma_G = \frac{M_G \cdot G^*}{w \cdot \Omega_G(G^*)} \tag{5}$$

As it can be observed, $\sigma_G$ is a dimensionless parameter that characterizes the external mass transfer (gas–liquid and liquid–solid) representing the ratio of the maximum possible mass-transfer rate to the maximum chemical reaction rate.

In order to quantify the intra-porous diffusional effects, the catalytic effectiveness factor ($\eta_C$) is used. It compares the observed reaction rate (in the presence of diffusional limitations) with the reaction rate calculated if the surface reactant concentration persisted throughout the interior of the catalyst particle. It can be expressed as:

$$\eta_C$$
$$= \frac{\text{actual over all reaction rate}}{\text{reaction rate without diffusional resistance, evaluated at the surface}} \tag{6}$$

When the reaction kinetics is nonlinear, as is usually the case for many of the catalytic reactions at industrial level, it is not possible to obtain an analytic solution for $\eta_C$. Froment and Bischoff [26] proposed an approximate analytical solution for nonlinear kinetics using the classic definition of $\eta_C$ for a first-order reaction modifying the definition of the Thiele modulus ($\phi$), which is determined by the following expression in the case of slab geometry:

$$\emptyset = L \cdot \rho_C \cdot \Omega_G(G_S) \cdot \left[2 \cdot \int_0^{G_S} D_e \cdot \Omega_G(G) dG\right]^{-1/2} \tag{7}$$

# 3 Theoretical derivation of the overall effectiveness factor for slab geometry

## 3.1 Langmuir–Hinshelwood kinetics

The kinetics can be expressed by a Langmuir–Hinshelwood (L–H) model. If the gas (usually hydrogen) is adsorbed associatively, the fraction of sites occupied by the gas will be defined by the following equation:

$$\theta_G^A = \frac{K_G \cdot G_s}{1 + K_G \cdot G_s} \tag{8}$$

The reaction rate for this compound will be given by:

$$\Omega_G = \frac{k_0 \cdot K_G \cdot G}{1 + K_G \cdot G} \tag{9}$$

$$R_G = \eta_c \cdot w \cdot k_0 \cdot \theta_G^A \tag{10}$$

Using the edible oil hydrogenation as an example of a typical three-phase reaction, $k_0$ has the following expression [19]:

$$k_0 = \frac{k_{MS} \cdot C_M + 2 \cdot k_{DM} \cdot C_{Di}}{2 \cdot C_{Di} + C_M + \frac{K_S}{K_M} \cdot C_S} \tag{11}$$

and $\eta_c$ is the catalytic effectiveness factor considering a slab geometry given by:

$$\eta_c = \frac{\tanh(\emptyset)}{\emptyset} \tag{12}$$

The Thiele modulus can be determined using the approximation proposed by Froment and Bischoff [26] (eq. 7), valid for reaction rates of general format. Performing the integration, we obtain

$$\emptyset = L \cdot \left(\frac{\rho_c \cdot k_{p1}}{D_e}\right)^{1/2} \\ \cdot \frac{K_G \cdot G_s}{(1 + K_G \cdot G_s) \cdot \{2 \cdot [K_G \cdot G_s - \ln(1 + K_G \cdot G_s)]\}^{1/2}} \tag{13}$$

where

$$k_{p1} = k_0 \cdot K_G \tag{14}$$

By substituting the expression of $G_s$ obtained in eq. (4) into eq. (13), the Thiele modulus can be formulated as a function of the effectiveness factor:

$$\emptyset = \frac{\emptyset_0 \cdot K_G \cdot G^* \cdot (1 - \eta/\sigma_G)}{\sqrt{2} \cdot [1 + K_G \cdot G^* \cdot (1 - \eta/\sigma_G)] \cdot \{K_G \cdot G^* \cdot (1 - \eta/\sigma_G) - \ln[1 + K_G \cdot G^* \cdot (1 - \eta/\sigma_G)]\}^{1/2}} \tag{15}$$

where $\emptyset_0$ and $\sigma_G$ can be expressed as:

$$\emptyset_0 = L \cdot \left(\frac{k_{p1} \cdot \rho_c}{D_e}\right)^{1/2} \tag{16}$$

$$\sigma_G = \frac{M_G \cdot (1 + K_G \cdot G^*)}{w \cdot k_{p1}} \tag{17}$$

$\sigma_G$ represents the ratio of the maximum mass-transfer rate to the maximum chemical reaction rate. $\emptyset_0$ denotes the ratio of the chemical reaction rate on the surface to the diffusion rate.

The overall effectiveness factor is obtained by substituting the expressions of rate $R_G$ (eq. 10), $\Omega_G$ (eq. 9), and $G_S$ (eq. 4) in eq. (1):

$$\eta = \frac{\eta_c \cdot (1 + K_G \cdot G^*) \cdot (1 - \eta/\sigma_G)}{1 + K_G \cdot G^* \cdot (1 - \eta/\sigma_G)} \tag{18}$$

As indicated in their corresponding definitions, $\eta$ and $\emptyset_0$ only depend on temperature through the variation of $K_G \cdot G^*$, $D_e$, $k_{p1}$, and $M_G$. They also depend on $\rho_c$ once the catalyst is selected.

Thus the value of $\eta$ is calculated by the trial-and-error method, after the parameters mentioned before are set. In the case of discontinuous stirred-tank reactors, the calculation of $\eta$ must be performed at each moment of progress of the reaction, for changes in the composition of the reactant mixture, changes in temperature or both simultaneously. For continuous stirred-tank reactors, $\eta$ has a unique value if the operation is carried out in the steady state.

In the case of plug-flow reactors operating under steady-state conditions, $\eta$ must be calculated for each axial section due to the change in the composition of reactants and products, the temperature at that particular section or both effects combined.

A plot of $\eta$ vs $\emptyset_0$ for different values of $\sigma_G$ (0.6 and 10) and $K_G \cdot G^*$ (0.1, 1, and 10) is presented in Figure 1, where it can be observed how the effectiveness factor increases with increasing $K_G \cdot G^*$. At the same time, the graph shows that for small values of $\emptyset_0$, the effectiveness factor tends to an asymptotic value. This observation corresponds to the region where the intraparticle diffusion resistance is negligible.

Following a similar approach to that developed above, but considering a dissociative gas adsorption on the catalytic surface, the fraction of occupied sites will be determined by:

$$\theta_G^D = \frac{\sqrt{K_G \cdot G_s}}{1 + \sqrt{K_G \cdot G_s}} \tag{19}$$

The Thiele modulus can be obtained similar to the previous case:

$$\emptyset = \frac{\emptyset_0 \cdot \sqrt{K_G \cdot G^* \cdot (1 - \eta/\sigma_G)}}{\sqrt{2} \cdot \left(1 + \sqrt{K_G \cdot G^* \cdot (1 - \eta/\sigma_G)}\right) \cdot \left\{K_G \cdot G^* \cdot (1 - \eta/\sigma_G) - 2 \cdot \sqrt{K_G \cdot G^* \cdot (1 - \eta/\sigma_G)} + 2 \cdot \ln\left(1 + \sqrt{K_G \cdot G^* \cdot (1 - \eta/\sigma_G)}\right)\right\}^{1/2}} \tag{20}$$
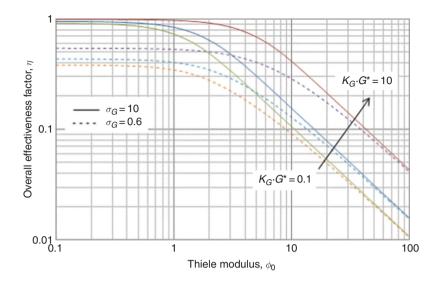
**Figure 1** Overall effectiveness factor for L–H kinetics with an associative gas adsorption mechanism in slab geometry. $K_G \cdot G^* = 0.1, 1,$ and 10

By substituting the $G_S$ (eq. 4) expression, we obtain

$$\emptyset = \frac{\emptyset_0 \cdot K_G \cdot G^* \cdot (1 - \eta/\sigma_G)}{\sqrt{2} \cdot [1 + K_G \cdot G^* \cdot (1 - \eta/\sigma_G)] \cdot \{K_G \cdot G^* \cdot (1 - \eta/\sigma_G) - \ln[1 + K_G \cdot G^* \cdot (1 - \eta/\sigma_G)]\}^{1/2}} \tag{21}$$

where $\emptyset_0$ is given by eq. (6), and $\sigma_G$ can be expressed as:

$$\sigma_G = \frac{M_G \cdot \sqrt{G^*}\left(1 + \sqrt{K_G \cdot G^*}\right)}{w \cdot k_0 \cdot \sqrt{K_G}} \tag{22}$$

The overall effectiveness factor is obtained by substituting the expressions of $R_G$, $\Omega_G$, and $G_S$ (eq. 4) in eq. (1):

$$\eta = \frac{\eta_c \cdot \sqrt{1 + K_G \cdot G^*} \cdot \sqrt{1 - \eta/\sigma_G}}{1 + \sqrt{K_G \cdot G^*} \cdot \sqrt{1 - \eta/\sigma_G}} \tag{23}$$

Similar to the case of associative gas adsorption, Figure 2 presents a plot of $\eta$ vs $\emptyset_0$ for different values of $\sigma_G$ (0.6 and 10) and $K_G \cdot G^*$ (0.1, 1, and 10) for the dissociative
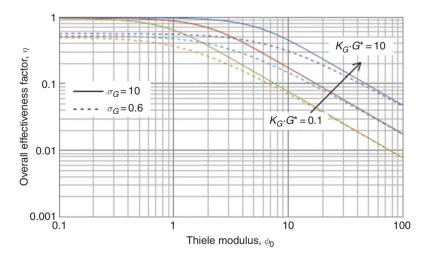


**Figure 2** Overall effectiveness factor for L–H kinetics with a dissociative gas adsorption mechanism in slab geometry. $K_G \cdot G^* = 0.1, 1,$ and 10

case. It can again be observed the typical behavior of the system under study.

## 3.2 Power law kinetics

When a reaction can be represented by power law kinetics, we have

$$\Omega_G = k_m \cdot G^m \tag{24}$$

$$R_G = \eta_c \cdot w \cdot k_m \cdot G_S^m \tag{25}$$

By rearranging eqs (4) and (25) and using the definition of the overall effectiveness factor, we obtain

$$\eta = \eta_c \cdot \left(1 - \frac{\eta}{\sigma_G}\right)^m \tag{26}$$

where $\eta_c$ is the catalytic effectiveness factor for slab geometry defined by eq. (12), and $\sigma_G$ is defined by eq. (5).

As expected, for the particular case where resistance to intraparticle diffusion is negligible, $\eta_c$ will be equal to the unit, therefore eq. (26) will be notably simplified.

The generalized effectiveness factor can be obtained using the Bischoff approximation, considering the type of kinetics according to the following expression:

$$\emptyset = L \cdot \left[\left(\frac{m+1}{2}\right) \cdot \frac{\rho_c \cdot k_m \cdot G_S^{m-1}}{D_e}\right]^{1/2} \tag{27}$$

This factor can be expressed in relation to the overall effectiveness factor using eqs (4) and (27):

$$\emptyset = \emptyset_0 \cdot \left(1 - \frac{\eta}{\sigma_G}\right)^{(m-1)/2} \tag{28}$$

where

$$\emptyset_0 = L \cdot \left[\left(\frac{m+1}{2}\right) \cdot \frac{\rho_c \cdot k_m \cdot (G^*)^{m-1}}{D_e}\right]^{1/2} \tag{29}$$

In order to apply the mathematical procedure, the power law kinetics for a three-phase reaction (half-order reaction) proposed by Hashimoto et al. [27] was used. As it was shown in preceding paragraphs, the graphical representation of the overall effectiveness factor vs $\emptyset_0$ can be used to calculate the reaction rate without having to turn into more complex calculations. Figure 3 represents the overall effectiveness factor in a plot of $\eta$ vs $\emptyset_0$ with $\sigma_G$ as parameter, with values equal to 1, 5, 10, 50, and 100.

## 3.3 Zero-order reactions

In three-phase reaction systems, the observed reaction rate can also be independent of the gas-phase concentration, and thus the reaction kinetics follows an apparent zero-order [20]. A procedure to calculate the effectiveness factor in reactions of this type for catalysts with spherical geometry was proposed [23, 28, 29]. By applying this method to monolithic systems, the overall effectiveness factor for slab geometry can be developed analogously.

According to this approach, there are two possibilities as shown in Figure 4: (A) the concentration of the gas inside the pores of the catalyst is never zero, in this case the reaction rates are not affected by the concentration
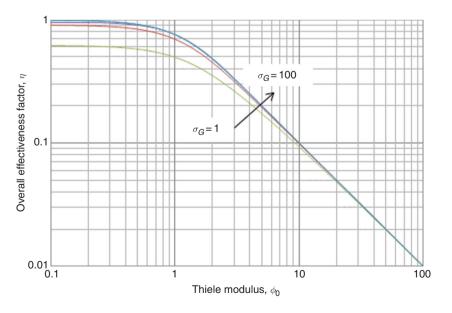


**Figure 3** Overall effectiveness factor for a half-order reaction applied to slab geometry. $\sigma_G = 1, 5, 10, 50,$ and 100
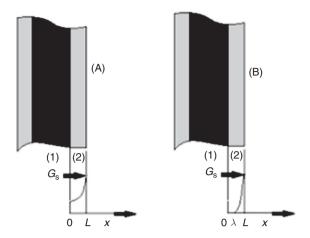
**Figure 4** Concentration profiles for a zero-order reaction, where the diffusional effects are: (A) negligible and (B) important. References: (1) monolith substrate and (2) porous support

profile, and the effectiveness factor is always 1; (B) the gas concentration becomes zero before reaching the end of the pore, and the effectiveness factor is always lower than 1.

The approaches to analyze the diffusion and reaction inside the pores of a spherical catalyst have been widely studied [30, 31]. Following an analogous analysis, the mass balance for a generic species $G$ inside the pores of a catalytic slab for a zero-order reaction is given by:

$$D_e \cdot \frac{d}{dx} \cdot \frac{dG}{dx} = k_0 \cdot \rho_c \tag{30}$$

where the boundary conditions are

$$\left\{ x = L; G = G_S \right\} \left\{ x = \lambda; \frac{dG}{dx} = 0 \right\} \tag{31}$$

The fact that the concentration of $G$ must be zero in longitude $\lambda$ is an additional restraint.

$$\left\{ x = \lambda; G = 0 \right\} \tag{32}$$

The solution to eq. (30) that satisfies the boundary conditions is

$$G = G_S + \frac{k_0 \cdot \rho_c}{D_e} \cdot \left[ \frac{x^2}{2} - \lambda \cdot x - \frac{L^2}{2} + \lambda \cdot L \right] \tag{33}$$

The value of $G_S$ at which the concentration falls to zero in the inner border of the catalyst layer is obtained by determining $\lambda = 0$ and $x = 0$ in eq. (33). This value is called $G_{S,crit}$ (stands for critical), and it is given by:

$$G_{S,crit} = \frac{k_0 \cdot \rho_c \cdot L^2}{2 \cdot D_e} \tag{34}$$

If under the operating conditions the value of $G_S$ is larger than $G_{S,crit}$, then the concentration inside the catalyst will

be finite at all points, whereas if $G_S < G_{S,crit}$, the concentration will be zero at some point called $\lambda$.

The global mass-transfer rate from the gas to the external surface of the solid is given by eq. (2). The rate of the chemical reaction when $G_S$ is greater than or equal to $G_{S,crit}$ is

$$R_G = w \cdot k_0 \tag{35}$$

where $k_0$ is defined by eq. (11) [19]. By eliminating $R_G$ in eqs (2) and (35), we obtain

$$G_S = G^* - w \cdot k_0 \cdot M_G^{-1} \tag{36}$$

Substituting this value of $G_S$ in eq. (34), we obtain the critical value of the concentration of $G$ in the liquid phase ($G_{crit}^*$) above which the concentration of $G$ is different from zero inside the catalyst under the studied operating conditions. This behavior can be expressed as:

$$G_{crit}^* = \frac{k_0 \cdot \rho_c \cdot L^2}{2 \cdot D_e} + w \cdot k_0 \cdot M_G^{-1} \tag{37}$$

If the concentration of $G$ in the liquid phase is greater than this critical value, there exist no mass-transfer limitations and the rate will be given by eq. (35). If $G^* < G_{crit}^*$, then the concentration would be zero at $x = \lambda$ inside the catalyst. The reaction only occurs in the region between $\lambda$ and $L$. Thus the rate is given by:

$$R_G = w \cdot k_0 \cdot \left[ 1 - \frac{\lambda}{L} \right] \tag{38}$$

Using the boundary condition (32), the value of $G_S$ can be expressed as:

$$G_S = \frac{k_0 \cdot \rho_c \cdot L^2}{2 \cdot D_e} \cdot \left[ \left( \frac{\lambda}{L} \right)^2 + 1 - 2 \cdot \frac{\lambda}{L} \right] \tag{39}$$

Substituting this value in eq. (2), we obtain

$$R_G = M_G \cdot \left[ G^* - \frac{k_0 \cdot \rho_c}{2 \cdot D_e} \cdot \left( \lambda^2 + L^2 - 2 \cdot L \cdot \lambda \right) \right] \tag{40}$$

In this case, the overall effectiveness factor is determined by the following equation:

$$\eta = \frac{R_G}{w \cdot k_0} \tag{41}$$

From eqs (38) and (41), we obtain

$$\eta = 1 - \frac{\lambda}{L} \tag{42}$$

If the process is entirely controlled by the gas–liquid and liquid–solid mass transfer, the reaction rate is
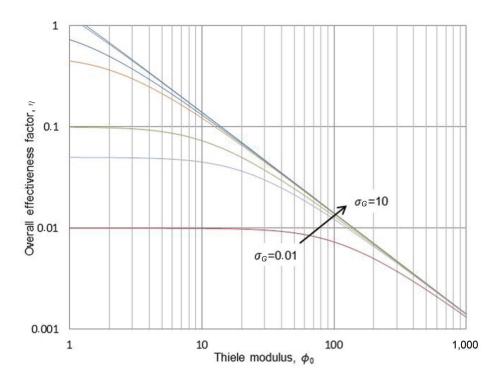
**Figure 5** Effect of the parameter $\sigma_G$ visualized in a plot of $\eta$ vs $\emptyset_0$ for a zero-order reaction in slab geometry

$$R_G = G^* \cdot M_G \tag{43}$$

The corresponding value for the effectiveness factor can be defined as a dimensionless parameter of external mass transfer:

$$\sigma_G = \frac{G^* \cdot M_G}{w \cdot k_0} \tag{44}$$

Dividing eq. (40) by $w \cdot k_0$ and rearranging it, we obtain

$$\eta = \sigma_G \cdot \left[ 1 - \frac{k_0 \cdot L^2 \cdot \rho_c}{2 \cdot D_e \cdot G^*} \cdot \left( \left( \frac{\lambda}{L} \right)^2 + 1 - 2 \cdot \frac{\lambda}{L} \right) \right] \tag{45}$$

Defining:

$$\emptyset^2 = \frac{k_0 \cdot L^2 \cdot \rho_c}{D_e \cdot G^*} \tag{46}$$

$$\frac{\lambda}{L} = 1 - \eta \tag{47}$$

The final expression for the effectiveness factor is obtained by the following equation:

$$\eta = \sigma_G \cdot \left[ 1 - \frac{\emptyset^2}{2} \cdot \left\{ 1 - 2 \cdot (1 - \eta) + (1 - \eta)^2 \right\} \right] \tag{48}$$

Eq. (49) is an implicit analytic equation where the effectiveness factor $\eta$ is expressed as a function dependent on $\sigma_G$ and $\emptyset^2$, which are defined by eqs (44) and (46). Eq. (48) can be represented graphically as a plot of $\eta$ vs $\emptyset$ with $\sigma_G$ as parameter. In this case, the values proposed for $\sigma_G$ were 0.01, 0.05, 0.1, 0.5, 1, 5, and 10 [28]. The value of $\eta$ can then be observed directly in Figure 5 without any other mathematical calculations. It is worth noting that parameters $\sigma_G$ and $\emptyset$ are fixed for a given process. Once $\eta$ is known, the reaction rate can be calculated using eq. (41).

# 4 Discussion

In order to analyze the theoretical results obtained for slab and spherical geometries, a direct comparison was made with the data reported by Ramachandran and Chaudhari [23], shown in Figures 6–10.

The results obtained for associative L–H kinetics, considering values of $K_G \cdot G^* = 0.1$, 1, and 10 with $\sigma_G = 10$, are presented in Figure 6. The same analysis was performed for $\sigma_G = 0.6$ and 5 (figures not shown). At higher values of $\sigma_G$, the external mass-transfer resistances are smaller. It can be observed that when the value of $K_G \cdot G^*$ increases, the overall effectiveness factor also increases. When analyzing constant $\emptyset_0$, it is observed that by favoring the kinetics (with higher values of $K_G \cdot G^*$) the internal transport also increased, and thus the effectiveness of the reactor (higher values of $\eta$). On the other hand, if $\sigma_G$ is constant and $K_G \cdot G^*$ increases, the external mass-transfer resistances decrease (according to the definition of $\sigma_G$) and $\eta$ increases.
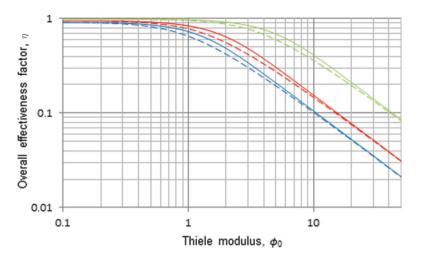
**Figure 6** Plot of $\eta$ vs $\emptyset_0$ for L–H type kinetics. Reference: Spherical geometry (solid line) and slab geometry (dotted line). For $\sigma_G = 10$, Reference: $K_G \cdot G^* = 0.1$ (blue), 1 (red), and 10 (green)

Being $K_G$ the adsorption constant of the gas in the active site, and $G^*$ the equilibrium concentration of the gaseous reactant in the liquid, the value of the parameter $K_G \cdot G^*$ is inherent to the system and it can be modified by changing the catalyst or the reaction system (gaseous reactant and/or liquid where it dissolves), and pressure and temperature, certainly.

Figure 7 shows the percent relative error for the overall effectiveness factor between spherical and slab geometries. The values of $K_G \cdot G^*$ mentioned above and $\sigma_G = 0.6$, 5, and 10 were considered. The combination of both parameters originated the nine curves presented in the figure. Maximum errors are observed at $\emptyset_0 \sim 2$ for $K_G \cdot G^* = 0.1$ and 1 and at $\emptyset_0 \sim 6$ for $K_G \cdot G^* = 10$.

In the conventional plots of $\eta_C$ vs $\emptyset_0$, it is observed that $\emptyset_0 \rightarrow 0$, $\eta_C \rightarrow 0$ for all the geometries, given that the kinetic effects are dominant in that zone. In the diffusion controlled area, $\emptyset_0 \rightarrow \infty$, $\eta_C \rightarrow 0$. In the mixed control area where the kinetic and diffusion effects compete $(^1/_3 < \emptyset_0 < 5)$, the geometry has a greater effect on $\eta_C$ [26].

For $\emptyset_0 \sim 2$, the smaller errors (~8%) were for the lower value of $\sigma_G$ (constant $K_G \cdot G^*$). In this case, the external mass-transfer resistances are important. The overall effectiveness factor involves the sum of the diffusional effects, both internal and external, and as the external effects are comparatively larger, the intraparticle transport loses importance, and consequently also the geometry. On the other hand, at higher values of $\sigma_G$ (5 and 10, with constant $K_G \cdot G^*$), the curves were closer and maximum errors were about 14% ($\emptyset_0 \sim 6$). When the external mass-transfer resistance was negligible (high values of $\sigma_G$), the
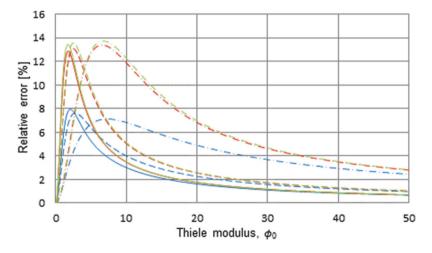


**Figure 7** Percent relative error for the overall effectiveness factor between spherical and slab geometries, corresponding to L–H type kinetics. Reference: $K_G \cdot G^* = 0.1$ (—), 1 (- - -), and 10 (-··-). $\sigma_G = 0.6$ (blue), 5 (red), and 10 (green)

maximum error found between the geometries tended toward the value of the catalytic effectiveness factor. The maximum difference between the catalytic effectiveness factors of the spherical and slab geometry was about 16%, and it occurred at $\phi_0 = 1.6$ [32].

When $\sigma_G$ remains constant, by increasing the value of $K_G \cdot G^*$, the external mass transport increases at the same time, as mentioned above, and this improvement in mass transport hides the geometric effects. For this reason, the maximum errors (greater differences between spherical and slab geometries) were observed at higher $\phi_0$ values, where the internal diffusion control begins to have more influence.

The percent relative error for the overall effectiveness factor between spherical and slab geometries with zero-order kinetics is presented in Figure 8. The values of $\sigma_G = 0.1$, $0.5$, and $1$ were considered. Maximum errors were found at $\phi_0 \sim 0.9$ (9%) for $\sigma_G = 1$ and 10 and at $\phi_0 \sim 2$ (4%) for $\sigma_G = 0.5$. The differences between geometries decreased when the external mass-transfer resistances increased. On the other hand, the maximum errors of the overall effectiveness factor corresponded to the differences between the catalytic effectiveness factors.

The percent relative error for the overall effectiveness factor between spherical and slab geometries with half-order kinetics is presented in Figure 9. Values of $\sigma_G = 1$,
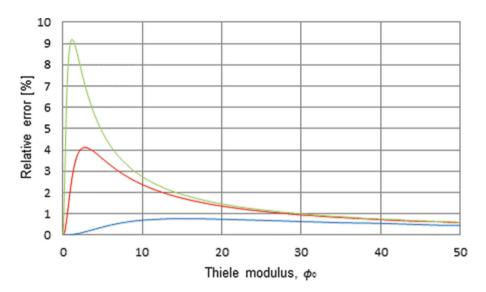


**Figure 8** Percent relative error for the overall effectiveness factor between spherical and slab geometries for zero-order kinetics. Reference: $\sigma_G = 0.1$ (blue), 0.5 (red), 1 (green)
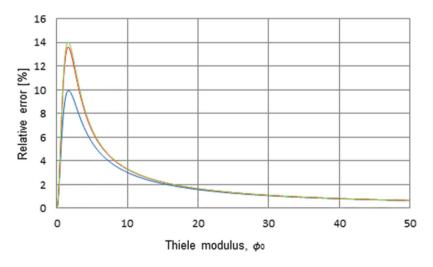


**Figure 9** Percent relative error for the overall effectiveness factor between spherical and slab geometries with half-order kinetics. Reference: $\sigma_G = 1$ (blue), 10 (red), and 100 (green)

10, and 100 were considered. The maximum errors were found at $\emptyset_0 = 1.7$ and were of ~10% for $\sigma_G = 1$ and ~14% for $\sigma_G = 10$ and 100. This plot exhibits the same trend presented in Figures 8 and 9.

# 5 Conclusions

Analytical solutions for the overall effectiveness factor for slab geometry applicable to uniform washcoats on a monolithic surface for three-phase reaction systems were obtained for zero-order reactions and L–H and power law kinetics. Implicit expressions for the overall effectiveness factor in terms of the Thiele modulus and external mass-transfer parameters were found.

The theoretical results were analyzed for a set of representative parameters, and it was observed that the errors resulting from not considering the geometry adequately reached values of up to 14% in procedures under mixed control (kinetic-internal diffusion) and negligible mass-transfer resistances.

In-depth knowledge of the behavior of a three-phase monolithic reactor operating under the studied working conditions would enable to make a detailed model of the system and optimize the process.

# Nomenclature

$a_L$ = Gas – liquid interfacial area per unit volume of liquid $\left[ m_{GL}^2/m_L^3 \right]$

$a_S$ = Liquid – solid interfacial area $\left[ m_{cat}^2/m_{cat}^3 \right]$

$C_j$ = Concentration of $j$ component, $j$ = Di, M, S [mol/m$^3$]

$D_e$ = Effective diffusivity [m$^2$/s]

$G$ = Concentration of G in the gas [mol/m$^3$]

$G^*$ = Concentration of G in the liquid in equilibrium with the gas [mol/m$^3$]

$G_S$ = Concentration of G at the catalyst surface [mol/m$^3$]

$k_0$ = Rate constant [mol/kg s]

$k_{DM}$ = Rate constant for the kinetic example in eq. (11) [mol/kg s]

$K_G$ = Adsorption equilibrium constant for G [m$^3$/mol]

$k_{GL}$ = Gas – liquid mass transfer coefficient $\left[ m_L^3/m_{GL}^2 \, s \right]$

$k_m$ = Rate constant for $m$th order reaction [mol/kg s]

$k_{MS}$ = Rate constant for the kinetic examplein eq. (11) [mol/kg s]

$k_{LS}$ = liquid – solid mass transfer coefficient [m/s]

$k_{P1}$ = Pseudo first order reaction rate order [m$^3$/kg s]

$K_S/K_M$ = Constant adsorption ratio [dimensionless]

$m$ = Order of reaction with respect to species G [dimensionless]

$M_G$ = Total mass transfer resistances [s$^{-1}$]

$R_G$ = Rate of reaction of Gperunit volume of reactor [mol/s m$^3$]

$w$ = Mass of catalyst per unit volume of reactor [kg/m$^3$]

$L$ = Thickness of the catalytic slab [m]

$x$ = Distance in the catalyst measured from the base of the pore [m]

## Greek letters

$\eta$ = Overall effectiveness factor [dimensionless]

$\eta_c$ = Catalytic effectiveness factor [dimensionless]

$\theta_G$ = Fraction of surface sites occupied bygas [dimensionless]

$\lambda$ = Distance from the center of the catalyst at which G concentration becomes zero [m]

$\rho_c$ = Density of the catalyst [kg/m$^3$]

$\sigma_G$ = Parameter defined by eq. (5) [dimensionless]

$\phi$ = Generalized Thiele modulus [dimensionless]

$\phi_0$ = Thiele modulus [dimensionless]

$\Omega_G$ = Local rate of chemical reaction perunit weight of catalyst [mol/kg s]

## Sub- and superscripts

A = Associative gas adsorption mechanisms

crit = stands for critical

D = Dissociative gas adsorption mechanisms

Di = Diene

M = Monoene.

S = Saturated

# References

1. Cybulski A, Moulijn JA. Monoliths in heterogeneous catalysis. Catal Rev Sci Eng 1994;36:179–270.

2. Irandoust S, Andersson B. Monolithic catalyst for non-automobile applications. Catal Rev Sci Eng 1988;30:314–92.

3. Kapteijn F, Nijhuis TA, Heiszwolf JJ, Moulijn JA. New non-traditional multiphase catalytic reactor based on monolithic structures. Catal Today 2001;66:133–44.

4. Boger T, Zieverink MM, Kreutzer MT, Kapteijn F, Moulijn JA, Addiego WP. Monolithic catalyst as an alternative to slurry systems: hydrogenation of edible oil. Ind Eng Chem Res 2004;43:2337–44.

5. Boger T, Roy S, Heibel AK, Borchers OA. Monolith loop reactor as an alternative to slurry reactors. Catal Today 2003;79–80:441–51.

6. Broekhuis RR, Machado RM, Nordquist AF. The ejector-driven monolith loop reactor: experiments and modeling. Catal Today 2001;69:87–93.

7. Bussard AG, Waghmare YG, Dooley KM, Knopf FC. Hydrogenation of alpha-methyl styrene in a piston oscillating monolith reactor. Ind Eng Chem Res 2008;47:4623–31.

8. Edvinsson-Albers RK, Houterman MJ, Vergunst T, Grolman E, Moulijn JA. Novel monolithic stirrer reactor. AIChE J 1998;44:2459–64.

9. Heiszwolf JJ, Engelvaart LB, van den Eijnden MG, Kreutzer MT, Kapteijn F, Moulijn JA. Hydrodynamic aspects of the monolith loop reactor. Catal Today 2001;56:805–12.

10. Irandoust S, Andersen B. Mass transfer and liquid-phase reactions in a segmented two-phase flow monolithic catalyst reactor. Chem Eng Sci 1988;43:1983–8.

11. Nijhuis T, Kreutzer M, Romijn A, Kapteijn F, Moulijn J. Monolithic catalysts as efficient three-phase reactors. Chem Eng Sci 2001;56:823–9.

12. Marwan H, Winterbottom JM. The selective hydrogenation of butyne-1,4-diol supported palladiums: a comparative study on slurry, fixed bed, and monolith downflow bubble column reactors. Catal Today 2004;97:325–30.

13. Boldrini DE, Sánchez JF, Tonetto GM, Damiani DE. Monolithic stirrer reactor: performance in the partial hydrogenation of sunflower oil. Ind Eng Chem Res 2012;51:12222–32.

14. Pérez-Cadenas A, Kapteijn F, Zieverink M, Moulijn J. Selective hydrogenation of fatty acid methyl esters over palladium on carbon-based monoliths: structural control of activity and selectivity. Catal Today 2007;128:13–17.

15. Sánchez JF, González Bello OJ, Montes M, Tonetto GM, Damiani DE. Pd/Al$_2$O$_3$-cordierite and Pd/Al$_2$O$_3$-fecralloy monolithic catalysts for the hydrogenation of sunflower oil. Catal Commun 2009;10:1446–9.

16. Sánchez MJ, Boldrini DE, Tonetto GM, Damiani DE. Palladium catalyst on anodized aluminum monoliths for the partial hydrogenation of vegetable oil. Chem Eng J 2011;187:355–61.

17. Machado R, Broekhuis R, Nordquist A, Roy B, Carney S. Applying monolith reactors for hydrogenations in the production of specialty chemicals-process and economic. Catal Today 2005;105:305–17.

18. Cordova WA, Harriot P. Mass transfer resistances in the palladium-catalyzed hydrogenation of methyl linoleate. Chem Eng Sci 1975;30:1201–6.

19. Fernández MB, Tonetto GM, Crapiste G, Damiani DE. Kinetics of the hydrogenation of sunflower oil over alumina supported palladium catalyst. Int J Chem Reactor Eng 2007;5:A10.

20. Santacesaria E, Parella P, Di Serio M, Borelli G. Role of mass transfer and kinetics in the hydrogenation of rapeseed oil on a supported palladium catalyst. Appl Catal A Gen 1994;116:269–94.

21. Tsuto K, Harriot P, Bischoff KB. Intraparticle mass transfer effects and selectivity in the palladium-catalyzed hydrogenation of methyl linoleate. Ind Eng Chem 1978;17:199–205.

22. Ramachandran PA, Chaudhari RV. Overall effectiveness factor of a slurry reactor for non-linear kinetics. Can J Chem Eng 1980;58:412–15.

23. Ramachandran PA, Chaudhari RV. Three phase catalytic reactors. New York: Gordon and Breach Science Publishers, 1983.

24. Sylvester D, Kulkarni AA, Carberry JJ. Slurry and trickle-bed reactor effectiveness. Can J Chem Eng 1975;53:313–16.

25. Ramachandran PA, Chaudhari RV. Theoretical analysis of reaction of two gases in a catalytic slurry reactor. Ind Eng Chem Proc Des Dev 1979;18:703–8.

26. Froment GF, Bischoff KB. Chemical reactor analysis and design. New York: Wiley, 1990.

27. Hashimoto K, Muroyama K, Nagata SJ. Kinetics of the hydrogenation of fatty oils. JAOCS 1971;48:291–5.

28. Chaudhari RV, Ramachandran PA. Influence of mass transfer on zero-order reaction in a catalytic slurry reactor. Ind Eng Chem Fundam 1980;19:201–6.

29. Chaudhari RV, Ramachandran PA. Three phase slurry reactors. AIChE J 1980;26:177–201.

30. Peterson EE. Chemical reactor analysis. New Jersey: Prentice Hall, 1965.

31. Wheeler A. Reaction rates and selectivity in catalysts pores. Adv Catal 1951;3:249–327.

32. Aris R. The mathematical theory of diffusion and reaction in permeable catalysts. London: Oxford University Press, 1975.